The UAVSAR Instrument: Description and Test Plans

Scott Hensley*, Kevin Wheeler*, Greg Sadowy*, Cathleen Jones*, Scott Shaffer*, Howard Zebker†, Tim Miller*, Brandon Heavey*, Ernie Chuang*, Roger Chao*, Ken Vines*, Kouji Nishimoto*, Jack Prater*, Bruce Carrico*, Neil Chamberlain*, Joanne Shimada*, Marc Simard*, Bruce Chapman*, Ron Muellerschoen*, Charles Le*, Thierry Michel*, Gary Hamilton*, David Robison*, Greg Neumann*, Robert Meyer*, Phil Smith*, Jim Granger*, Paul Rosen*, Dennis Flower* and Robert Smith‡

* Jet Propulsion Laboratory, 4800 Oak Grove Drive, Pasadena, CA 91109

Email: scott.hensley@jpl.nasa.gov

†Stanford University, Palo Alto, CA 94305

‡Goddard Space Flight Center, Greenbelt, Maryland, 20771

***Abstract*— The UAVSAR instrument had its genesis in the ESTO Instrument Incubator Program and after 2.5 years of development is nearing readiness to collect engineering and science data. System design was motivated by solid Earth applications where repeat pass radar interferometry can be used to measure subtle deformation of the surface, however flexibility and extensibility to support other applications were also major design drivers. By designing the radar to be housed in an external unpressurized pod, it has the potential to be readily ported to many platforms. Initial testing is being carried out with the NASA Gulfstream III aircraft, which has been modified to accommodate the radar pod and has been equipped with precision autopilot capability developed by NASA Dryden Flight Research Center. With this the aircraft can fly within a 10 m diameter tube on any specified trajectory necessary for repeat pass radar interferometric applications. To maintain the required pointing for repeat-pass interferometric applications we have employed an actively scanned antenna steered using INU measurement data. This paper presents a brief overview of the radar instrument, and the testing conducted to date to validate its functional and performance requirements.**

I. Introduction

Earth science research often requires crustal deformation measurements at a variety of time scales, from seconds to decades. To meet these needs, the NASA Solid Earth Science Working Group has recommended an observational program that includes both airborne and spaceborne capabilities, and this is reflected in the NASA Earth Science Enterprise strategic plan. Since many geophysical processes, such as volcanic eruptions and earthquake events, occur quickly and require near-immediate response by scientists and disaster managers alike, the goal is to provide Earth deformation measurements on an hourly basis with global access. While this objective is best supported by a spaceborne high-orbit (e.g. geosynchronous) constellation of repeat-pass interferometric SAR satellites, the recommended first step in this observational program is a low-earth-orbit deformation satellite with a repeat period of roughly one week. The sub-orbital radar program enters the Earth Science Enterprise plan as a key supplemental capability delivering the short time baseline observations, and providing repeat-pass measurements at time scales much smaller than one week, potentially as short as twenty minutes.

Understanding the time varying nature of rapidly deforming features such as basaltic volcanoes and glaciers or deformation from post seismic transients requires observational sampling intervals of a day or less to capture and model transient events. In addition to providing unprecedented temporal detail of deformation of dynamic processes, the suborbital radar will be a testbed for understanding the observational needs for how rapid repeat observations would be acquired. This is a capability that the current operational NASA AIRSAR system has demonstrated but cannot practically support for science experiments in its current configuration due to lack of track repeatability and beam pointing limitations.

Although satellites have been used for repeat-track interferometric (RTI) SAR mapping for close to 20 years, repeat track interferometry is much more difficult to implement from an airborne platform, [7]. Aircraft motion compensation methods have until recently not been sufficiently accurate to recover cm-scale deformations, and existing radar systems were designed without the necessary controls on flight position and antenna pointing to support repeat-pass InSAR. In fact, several organizations have acquired experimental airborne RTI data, but these lack the capability to acquire significant amounts of scientifically useful RTI data. The primary technical reasons for this state of affairs remain: 1) it is difficult to fly the same or nearly the same pass twice in the troposphere, due to wind gusts, turbulence, etc., and 2) it is difficult to maintain the same antenna pointing on repeated passes due to varying cross-winds that lead to varying yaw angles. The UAVSAR system is specifically designed to overcome these limitations and produce high-quality RTI maps routinely.

The UAVSAR project will also serve as a technology test bed. As a modular instrument with numerous plug-and-play components, it will be possible to test new technologies for airborne and spaceborne applications with relatively little difficulty. Joint experiments with other radar instruments, for example radars flying in formation with an active link between platforms, can also be accommodated without redesign of the system. In fact, several experiments have been proposed at

Fig. 1. *Modified NASA Gulfstream III in early flight tests with the UAVSAR pod attached to the underside of the aircraft. Photo courtesy of NASA Dryden Flight Research Center.*

different frequencies that make use of the modular design of the system.

II. Instrument Design

Making robust repeat-pass radar interferometric measurements at L-band to measure both natural and anthropogenically induced deformation of the Earth's surface from an airborne platform presents difficulties not found in spaceborne observations due to the above mentioned navigation and pointing constraints. The UAVSAR radar is designed from the beginning as a miniaturized polarimetric L-band radar for repeat-pass and single-pass interferometry with options for along-track interferometry and additional frequencies of operation. The radar will be initially deployed on the NASA Gulfstream III aircraft with the potential to be ported to other aircraft such as the Predator or Global Hawk UAVs. Figure 1 shows the instrument pod attached to the underside of the NASA Gulfstream III during early flight testing of the aircraft modifications. Key measurements the system has been designed to make in support of various NASA science programs include:

- Precision crustal deformation for monitoring earthquakes both during and after a seismic event, for monitoring volcanic activity and for monitoring human-induced surface change such as subsidence induced by oil or water withdrawal, or other displacements of the surface from human activities.
- Polarimetric interferometry, which can provide measurements of forest structure and sub-canopy topography.
- Polarimetric tomography, mapping in detail the vertical structure of a vegetated area.

Robust repeat-pass radar interferometric measurement needs impose two observational constraints on the UAVSAR radar and system. First, it is necessary that on repeat observations the aircraft fly within a specified distance of its previous flight trajectory. UAVSAR has a science-derived requirement for flight track repeatability of 10 m, hence NASA Dryden has modified the NASA Gulfstream III to include a Precision Autopilot capability [5] to control aircraft position. The precision autopilot uses input from the real-time DGPS (discussed in Section II-C) to generate signals that are used to drive the aircraft's ILS landing system. Early flight tests indicate that this requirement will be met. Secondly, it is also essential that the antenna look directions are identical within a fraction of the beamwidth. Because the wind can be substantially different at different times, even if the platform is capable of accurately repeating the desired track, the yaw angle of the aircraft can vary widely on different tracks due to different wind conditions aloft. UAVSAR thus employs an electronically steered flush mounted antenna that is pointed in the desired direction based on real-time attitude angle measurements. As such, the UAVSAR system is a tight blending of platform and sensor capabilities.

TABLE I
Radar Parameters

Parameter	Value
Frequency	1.26 GHz (.2379 m)
Bandwidth	80 MHz
Pulse Duration	5-50 μs
Polarization	Quad Polarization
Range Swath	16 km
Look Angle Range	$25^\circ - 65^\circ$
Transmit Power	3.1 kW
Antenna Size	0.5m $\times$ 1.6 m
Operating Altitude Range	2000-18000 m
Ground Speed Range	100-250 m/s

Other technological factors also influenced the design, extending the usefulness and expandability of the initial system. The philosophy of the radar design is as follows: The design should be modular, compact, light-weight, and adaptable to the NASA Gulfstream III as well other airborne platforms including UAVs. The design should also be flexible so that this radar platform can serve as a testbed to demonstrate new radar technology and techniques. Based on the science objectives and the platform characteristics, the key parameters of the radar design are given in Table I. In the following sections, we will outline the radar design for the L-band polarimetric RPI radar and its expected performance.

Figure 2 shows a block diagram of the UAVSAR radar. After a brief overview of the block diagram each of the subsystems is discussed in further detail. The radar has been designed to minimize the number of interfaces with the aircraft for improved portability. The aircraft provides 28 V DC power to the radar via the Power Distribution Unit (PDU), which is also responsible for maintaining the thermal environment in the pod, and the radar provides its real-time DGPS position data to the aircraft for use by the Precision Autopilot. Waypoints for the desired flight paths are generated prior to flight by the Flight Planning Subsystem (FPS) and loaded into the Precision Autopilot and into the radar's Automatic Radar Controller (ARC) along with radar command information for each waypoint. The ARC is the main control computer for the radar and controls all major functions of the radar during flight. It is designed to operate in a fully autonomous mode or to accept commands from the Radar Operator Workstation (ROW) either through an ethernet connection on crewed platforms or through

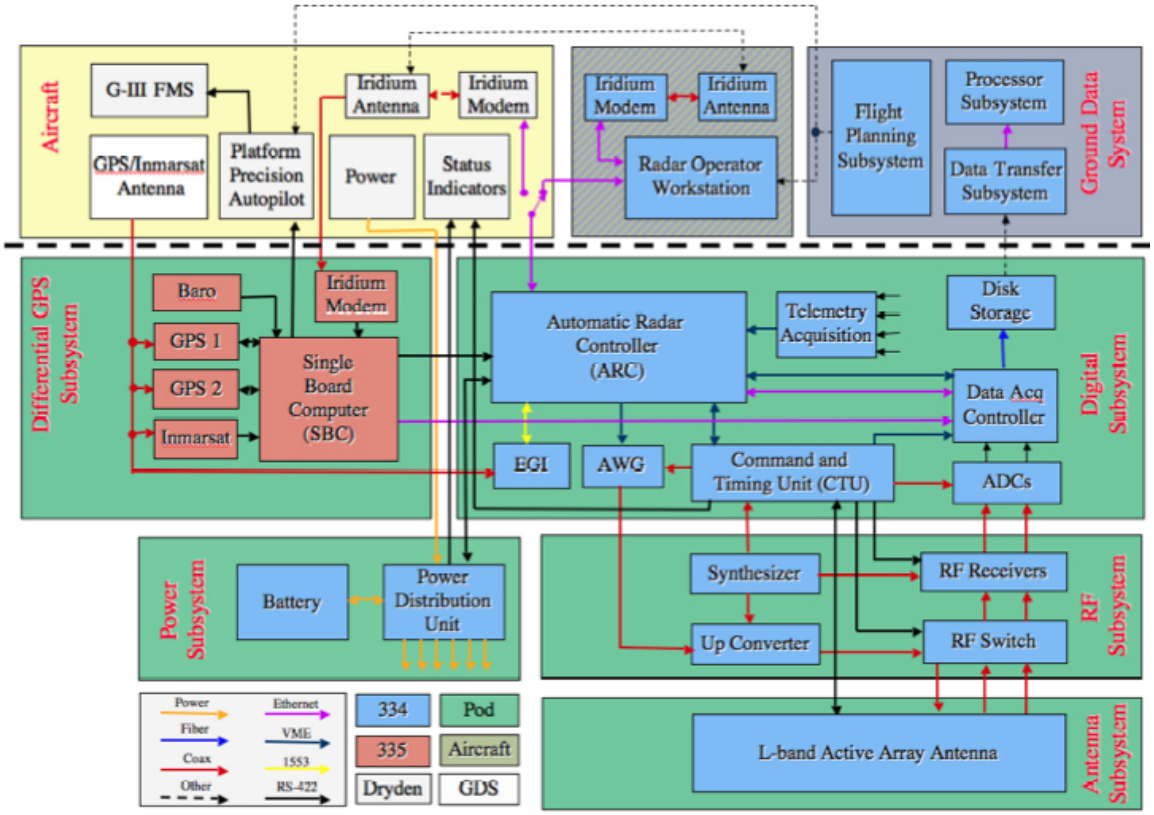

Fig. 2. *UAVSAR Radar Block Diagram, including aircraft, real-time differential GPS, and ground system interfaces. Color is used to code the various signal and control paths for the radar as indicated at the bottom left of the figure. The Iridium communication system can be used to communicate with the radar and GPS systems while in flight.*

an Iridium modem for uncrewed platforms. The Control and Timing Unit (CTU) controls the timing of all the transmit and receive events in the radar timeline and thus interacts with many of the radar digital and radio frequency (RF) electronics. The active array antenna consists of 24 130 W L-band Transmit/Receive (TR) modules that feed 48 radiating elements within the 0.5 m by 1.5 m array. Figure 3 illustrates how the various electronic subsystems are arranged within the pod.

A. Weight and Power

The system requires just under 2 kW DC power when the radar is transmitting L-band polarimetric RPI . This is well within the capacity of the Gulfstream III aircraft and many other platforms considered for hosting the UAVSAR radar. The standby DC power is on the order of 150 W. The active array antenna weighs less than 50 kg; each T/R module weighs about 0.5 kg. The remainder of the radar electronics in the payload bay weighs less than 100 kg (approximately 20 kg for the RFES, 30 kg for the DES, and 30 kg for cabling, power distribution, etc.) for a combined instrument weight of less than 230 kg.

B. Digital Electronics Subsystem

The Digital Electronics Subsystem (DES) provides the overall timing and control signals for the radar as well as the telemetry and data acquisition functions. All the digital units are housed in a custom built VME card cage. Coordination and control of all the radar subsystems is through the master computer for the DES, the ARC. The ARC flight software controls the UAVSAR system for both attended and unattended flight operations. The ARC can be operated in two primary modes, manual mode and automatic mode. In manual mode a radar operator selects the mode and operating parameters for the radar using a menu driven GUI on the ROW. In automatic mode the ARC tracks the aircraft trajectory using data from the inertial navigation unit (INU) and initiates power state transitions, data take start and end and other housekeeping functions based on proximity to predefined waypoints uploaded from the ROW prior to flight. In many respects the ARC flight software must perform duties normally associated with spaceflight missions. This includes the ability to collect science data without operator intervention and to perform fault monitoring and recovery to minimize loss of mission objectives during flight. The ARC flight software utilizes the Wind River vxWorks operating system, a preemptive hard real-time kernel used by many flight projects at JPL. The ARC flight software is interrupt driven and has stringent performance requirements. In addition to commanding the radar timing unit during science data collection, the ARC flight software handles the Embedded GPS/INU telemetry collection, tracks the aircraft flight path, performs electronic beam steering calculations, updates attenuation parameters and monitors temperatures inside the pod. The ARC software is

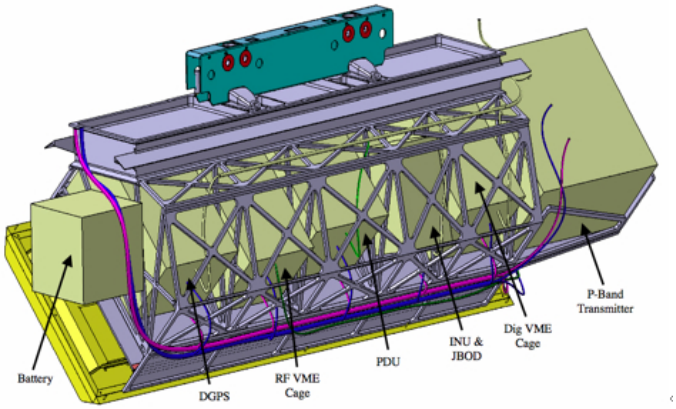

Fig. 3. *Diagram showing the location of the various electronic packages within the pod.*

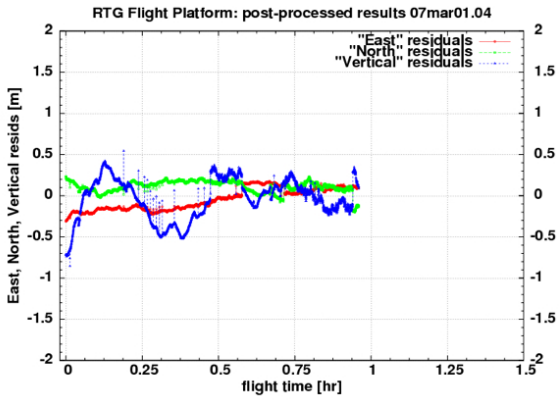

Fig. 4. *Flight testing of the engineering model of the real-time DGPS show that it is easily meeting its 1 m tube requirements with the east, north and vertical residuals shown in the plot.*

being validated as part of system integration and test.

Precision timing of the pulse generation, ADC operation and antenna commanding are essential for proper radar operation. As the UAVSAR radar can operate in a number of complex modes including multi-polarization, multi-frequency and multi-antenna modes of operation, the CTU unit which controls all the precision timing was custom built at JPL using a Xilinx FPGA. The CTU provides receiver gains to the RFES based on commands sent from the ARC and provides a receiver protect signal to shut off the sensitive radar receivers during pulse transmission. Additionally, the CTU generates all the radar timing signals for the Arbitrary Waveform Generator (AWG), antenna, radar receivers and the data acquisition. All key radar events are time tagged by the CTU and recorded in the data header for subsequent processing.

Shared use of the frequency spectrum is getting more complicated as the number of applications and users continues to increase. As radars designed for specific science applications are driven by physics to operate in selected frequency bands, it is becoming more necessary to adjust our transmitted waveforms to be compatible with other users of the spectrum. This is particularly true for lower frequency radars operating in the P and VHF bands. To provide the desired waveform flexibility JPL designed and built a custom AWG. The AWG is a conduction cooled 6U VME card that has two independent waveform generators on the card. The AWG provides flexibility in pulse width, pulse repetition frequency and waveform design supporting bandwidths up to 200 MHz in a compact, light weight and low power consumption module.

After each transmitted pulse the radar opens a receive window and digitizes the return signal. The radar employs an offset video sampling scheme (i.e. records real instead of complex samples) and to meet Nyquist sampling rate criteria samples the data at 180 MHz, which is more than twice the radar bandwidth of 80 MHz. With pulse repetition rates up to 1 KHz per data channel and receive window durations up to 150 μs, the radar generates large volumes of data. The ADC board is a 12 bit conduction cooled 6U VME card that is a commercial off-the-shelf board from Pentek. Onboard data rate reduction uses an optional Block Floating Point Quantization (see [4]) algorithm where the user selects how many bits are retained for each data sample, anywhere between 12 and 2 bits. Dynamic range is maintained by supplying an exponent for each group of 128 samples (this can be set by the user) called a block. BFPQ is implemented on a back-end FPGA on the Pentek board.

After the returned data is digitized and possibly data compressed in the ADC board, it is buffered in the Data Acquisition Controller (DAC) along with an ancillary header and time tag data from the ARC and CTU. Information embedded in the header includes radar command parameters (e.g. PRF, gains, starting range, etc.), navigation data (e.g. position, velocity, attitude angles, etc.), time tags (both radar and GPS) and various data identification information. Raw signal and header data, as well as other ancillary files including GPS raw data file, data from the INU and a flight log file are stored onto a disk array called a JBOD (just a bunch of discs). The SANBric JBOD is a hermetically sealed commercial off-the-shelf storage device with a capacity of 1.8 TB manufactured by Vmetro.

C. Navigation Subsystem

Repeat-pass radar interferometry requires highly accurate ephemeris and attitude information in real-time for flight path control, steering the electronic scanned antenna and for post processing of the SAR image data. UAVSAR's navigation subsystem consists of a real-time differential GPS and a commercial off-the-shelf INU. The real-time DGPS is a custom box developed by JPL that is a blend of commercial off-the-shelf components in a customized housing coupled with specialized software hosted on a single board computer. Data from NavCom and Ashtech (Magellan) GPS Receivers are blended with real-time correction data, broadcast via Inmarsat and Iridium satellite networks. While standard GPS position accuracy is 5-10 m, the UAVSAR DGPS uses correction information and JPL's Real-Time GIPSY software to achieve sub-meter precision. Figure 4 shows that the engineering model easily met the 1 m real-time requirement and the flight unit is expected to perform similarly. The INU is a Litton LN-251, which is an integrated INU/GPS system that provides

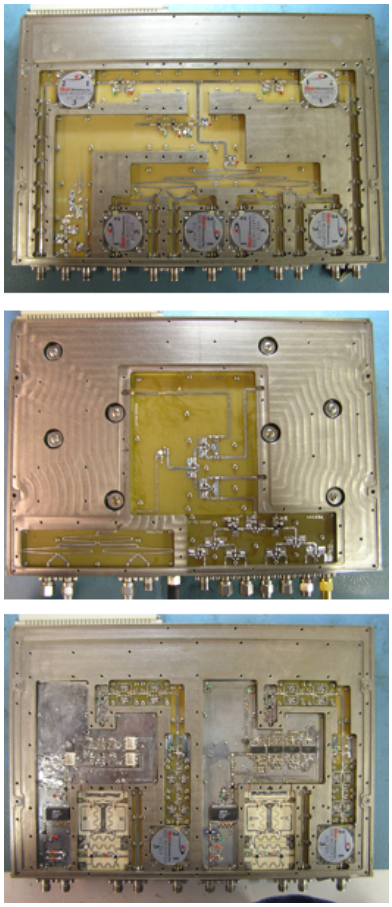

Fig. 5. *Photographs of the three units that make up the radar RFES supplied by Artemis. The top unit is the upconverter, the middle unit is the frequency synthesizer and the bottom unit is the dual receiver.*

high accuracy position, velocity and attitude data at a 50 Hz rate. Data from the DGPS and INU are blended post-flight in the ground data system to generate the position and attitude data used to process the SAR data.

D. RF Subsystem

The Radio Frequency Electronic Subsystem (RFES) consists of three custom built units by Artemis, Inc. that are housed in a custom VME cage. The frequency synthesizer provides a 10 MHz reference signal for frequency generation, supplies a local oscillator (LO) signal for the upconverter and receivers, and a timing signal for the AWG. Upconversion of the baseband AWG center frequency of 137.5 MHz to the desired transmit center frequency of 1257.5 MHz and routing of the signals to the antenna switch network or receivers, as appropriate, are done in the upconverter unit. Dual L-band receivers take the returned signal from the H and V polarization channels and translate the L-band echo data down to 45 MHz prior to injection into the ADCs. Figure 5 shows the three RF units with their covers removed.

E. Antenna Subsystem

The antenna subsystem consists of an electronically-scanned phased array which allows the beam to be scanned along track to compensate for any aircraft yaw that differs from pass to pass in interferometric measurement mode. The antenna is composed of 48 (12 along track, 4 across track) patch radiating elements that are fed by 24 transmit / receive (TR) modules. Each module feeds a pair of patches in a column of four with the outer patches being fed at level 10 dB below the power level of the inner patches. This taper provides the wide beamwidth in the cross-track direction that is required for a large measurement swath and also suppresses sidelobes which otherwise lead to multipath from the aircraft wing.

The patch array is implemented in six tiles of eight patches each. Each tile is composed of a radiating patch layer made from Rogers RT/Duroid 6002 material, a low dielectric layer made from Astroquartz honeycomb and a stripline divider layer also made from RT/Duroid 6002. These materials were chosen for their RF performance and their excellent mechanical and electrical stability over temperature. Each patch is symmetrical and has orthogonal balanced feed points so that V and H polarization can be transmitted and received with good polarization purity. The stripline layer contains feed networks for both polarizations, including edge couplers to provide the 10 dB taper and 180 degree hybrids to provide balanced patch feeds.

The six radiating tiles are bonded to an aluminum honeycomb structure with their RF connectors protruding through holes in the structure. The rear side of the aluminum honeycomb panel carries all of the active electronics including TR modules, the Energy Storage Subsystem (ESS), RF manifolds, an Antenna Switch Network (ASN), TR and Antenna switch network Controller (TRAC) and DC/DC converters. Figure 6 shows a view of the backside of the antenna with 8 of the 24 TR modules populating the array.

The TR modules (produced by REMEC Defense and Space) each contain a transmitter supplying approximately 130 W, and two receivers. All three channels have controllable phase and the receiver channels also have controllable gain. A calibrated phase and amplitude lookup table is loaded into each module prior to each data take. During the data take, the ARC uses information from the INU to continuously command the beam to be perpendicular to the current flight track. Upon receiving a steering command, each module looks up the calibrated phase values for that particular scan direction and loads them into its phase shifters and programmable attenuators. The calibrated lookup table compensates for feed path length errors due to a module's position in the array and the measured temperature variation of that particular module, generating a nearly ideal aperture distribution for the desired scan angle.

The RF signals are distributed to and combined from the TR modules using stripline corporate networks implemented in three 9-layer RT/Duroid 6002 manifold boards. The upper and lower antenna halves have separate networks and there are separate networks for transmit, receive H, receive V, and calibration yielding a total of eight 12-way networks. All eight networks connect to the antenna switch network which allows the two receiver outputs to be connected to the H and V receivers of the full antenna or to the upper or lower halves of

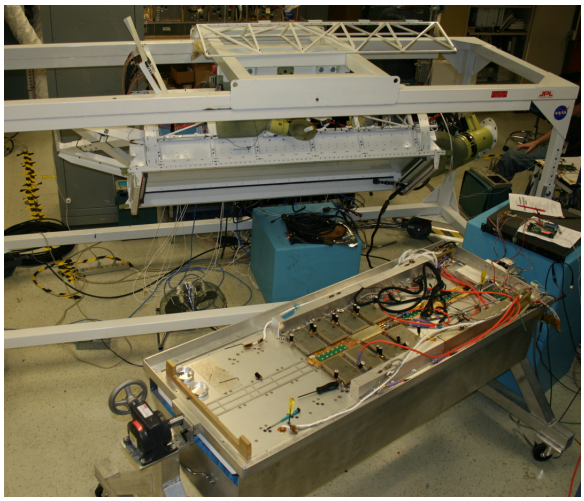

Fig. 6. *View of the backside of the antenna with 8 TR modules undergoing tests within the array. In the background is the UAVSAR pod with the mounting location of antenna easily visible.*

the antenna for either H or V. The ASN also allows loopback of calibration signals directly back to the receiver or through the TR modules.

The antenna subsystem is designed to receive unconditioned 28 V power from the aircraft and generate the voltages required for operation of its subassemblies. 9 V and -28 V power is generated by high-reliability COTS DC/DC converters, while the pulsed 31 V power required for the transmitters is supplied by six Energy Storage Subsystems. The ESS is a custom DC-DC converter with substantial charge storage and very low series resistance. This allows it to supply pulses of greater than 50 A with little voltage sag, minimizing transmitter power droop over the pulse.

F. Power Distribution Unit

By electing to have a pod based radar sensor in an unpressurized pod to facilitate future transition to other platforms, the sensor design incurred a more complicated thermal control scenario. The power distribution unit is a custom JPL design that includes a Complex Programmable Logic Device (CPLD) for the thermal control algorithm as well as provisions for taking the aircraft 28 V DC power and distributing to the various electronic subsystems. Temperature control for active array and radar electronics is accomplished using a combination of heaters and louvers that control the amount of air flowing through the cooling ducts. Separate ducts and louver control are provided for the radar electronics, the active array antenna, and the JBOD. Thermal sensors mounted at strategic points throughout the electronics and active array are monitored once per second by the PDU, which adjusts the louver position or the on/off state of the heaters to keep each radar unit in its appropriate temperature range. It is extremely to maintain the temperature units above the dew point during descent to prevent condensation on the electronics. Desired temperature ranges are stored in tables uploaded from the ROW through the ARC to the PDU. Figure 7 shows a functional block diagram of the thermal control algorithm.

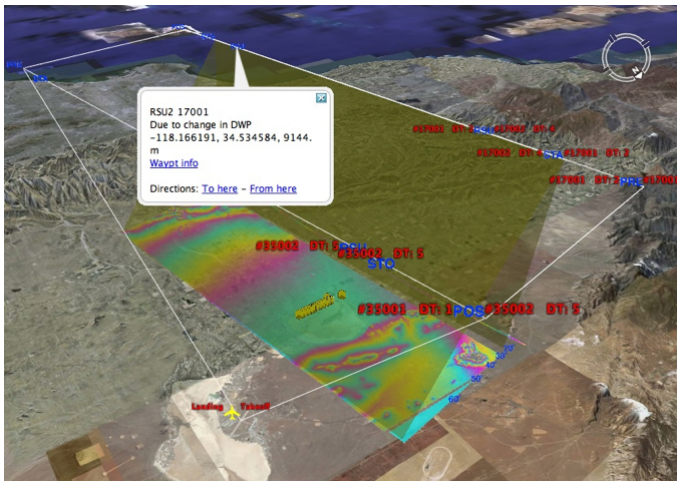

Fig. 8. *Output of the UAVSAR flight planning tool in Google Earth™ from the UAVSAR flight planning tool. The tool allows the user to see the planned swath to be mapped, look angles within the swath, display waypoint and designated target information, and the planned aircraft flight trajectory.*

Two test flights of the PDU and the thermal control algorithm have been conducted with the pod populated with dummy masses in place of the other radar units. The flight profile for these tests included level flight at various altitudes and speeds to ascertain the algorithm performance in a variety of conditions. These tests indicated that the PDU and thermal control algorithm are working nominally, however we found that additional sealing of the pod was needed to prevent unwanted airflow from over cooling the units in flight. Some of these modifications were made prior to the second flight resulting in much improved thermal control.

G. Flight Planning Subsystem

In order to maximize science return and accommodate the autonomous nature of radar operations, a flexible and powerful flight planning and visualization tool has been developed. The flight planning tool takes inputs on the desired trajectory characteristics, terrain types to be imaged, targets of interest, desired radar mode of operation for all the flight lines for a particular sortie and generates a flight plan file which is uploaded to the ARC containing the information required to collect the desired science data. Outputs of the tool include waypoints along the trajectory, starting and ending ranges in the data window, gain settings for the various polarization channels and desired antenna steering angle information. In order to make the information easily digestible by the science investigators, the tool outputs a KML file that can be read by Google Earth™ to display all the relevant information visually. Figure 8 shows the output of the flight planning tool for our test site at Rosamond Lake Bed in the Mojave Desert of California. The tool allows the user to see the planned swath to be mapped, look angles within the swath, display waypoints and designated target information (with additional data available by clicking on the point), and the planned aircraft flight trajectory.

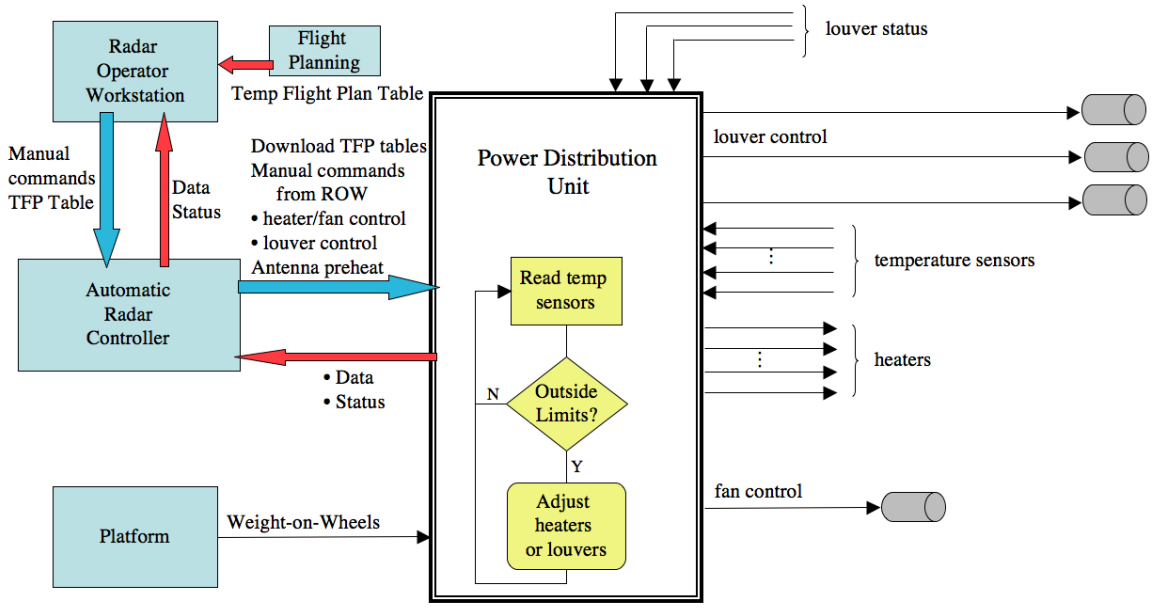

Fig. 7. *This figure shows a functional block diagram of the thermal control algorithm that is a part of the PDU subsystem.*

H. Ground Data Subsystem

Repeat-pass airborne radar interferometry requires sophisticated processing algorithms to generate the desired deformation and associated science data products. The UAVSAR Ground Data System (GDS) consists of the hardware and software necessary to process and archive UAVSAR raw science data and the derived science products.

1) Data Transfer: Science data and various ancillary files for each datatake are stored on the JBOD during flight. Subsequent to landing, data are transferred from the JBOD to another storage media to ready the JBOD for another flight. The removed unit is replaced with an another JBOD so that sorties occurring in less than the data transfer time can be supported. The Data Transfer Subsystem (DTS) is hosted on an HP ProLiant ML350 G4p equipped with 2 GB of RAM. Two copies of the science data are nominally transferred from the JBOD to LTO-3 tape. One copy can then be shipped to JPL while the other is kept in reserve until the tapes arrive at JPL and are archived. Average data transfer rate from the JBOD to tape is 75 MB/s (145 MB/s from JBOD to disk) so 1.8 TB can be transferred in approximately 10.5 hours. If a full byte for byte verification of at least one tape copy is performed then the data transfer time is 19 hours.

2) Motion Processing: Precise knowledge of the antenna location for each pulse is necessary for radar interferometric data processing. The motion processing software blends data from the INU and DGPS and converts the blended ephemeris data into a suitable coordinate system for radar signal processing. Blending is done using a Kalman filter followed by a fixed-interval smoother to get the high position accuracy of the DGPS coupled with the high temporal resolution provided by the INU in a globally optimal solution to the platform position using all available measurement data. Additionally, the algorithm includes provisions for precisely linking the motion data to the pulse data via information put in the science data headers by the CTU. Outputs of the motion processing software include the filtered and reformatted ephemeris data, files that link the pulse data to the motion data and command files to run the image formation processor.

3) Image Formation, Interferometric and Science Processing: Generation of image and science data products follows motion processing. Figure 9 shows the major steps of the processing methodology for differential airborne repeat-pass interferometry. After the motion processing step is completed for a repeat-pass pair of images, a subsequent motion alignment algorithm is employed to determine proper processing parameters for the science data so that the imagery will be co-aligned in both the along-track and cross-track directions. Also, a common coordinate system and reference path based on the two trajectories is selected. Data for both passes are then processed through the image formation processor to generate single look complex (SLC) imagery. If the ephemeris knowledge were perfect then the two images would be co-registered precisely. However, even with the best post processing of the DGPS data, the expected relative position accuracy between the two passes is on the order of 2-3 cm, an order of magnitude or more larger than the required accuracy to achieve the fraction of a pixel offset that is required for interferometric applications. To achieve improved alignment the relative position data, called the baseline, is refined based on the SLC images themselves. Several methods exist for recovering residual motion. These differ in implementation and accuracy, however the basic idea is to use the mis-registration information between the SLC images to derive a baseline correction. After the residual baseline is estimated the improved ephemeris is used to reprocess the data. The procedure may be repeated until the two images are co-registered with sufficient accuracy.

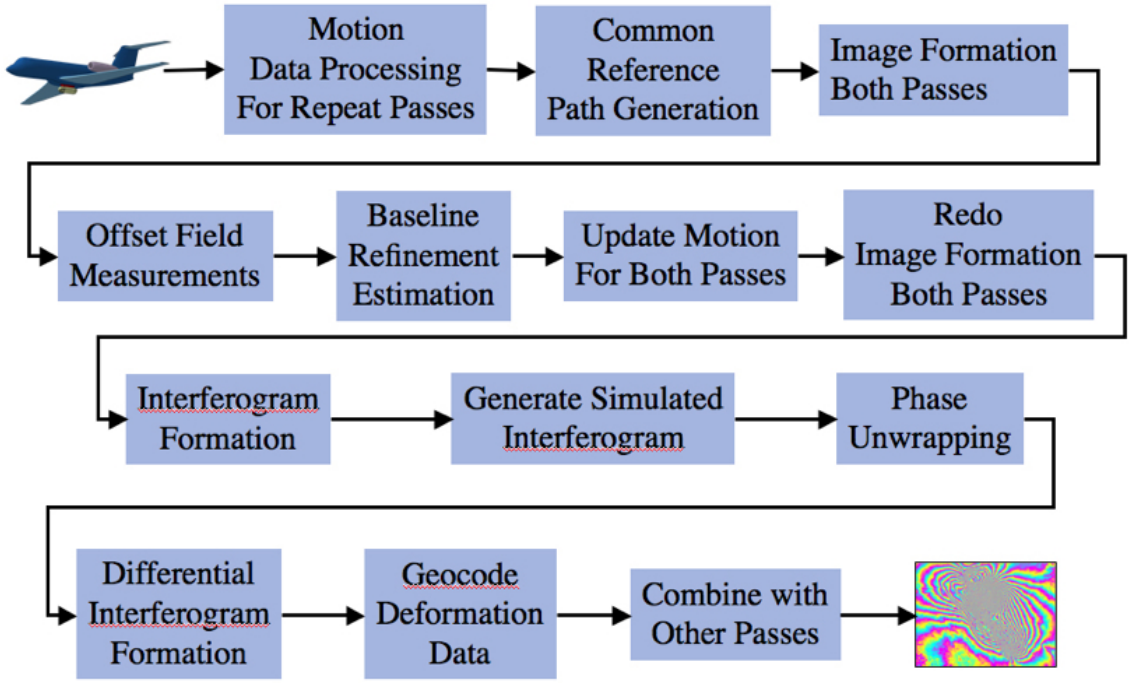

Fig. 9. *Processing methodology for differential interferometry for airborne RTI. Unlike processing of spaceborne RTI data, where the flight path is very smooth over time such that residual errors can be easily modeled after initial processing, airborne flight tracks are not known sufficiently well in advance. It is necessary to use the data themselves to refine the time-varying the baseline between flight tracks, reprocess the data with updated flight track information, then proceed with interferometric processing.*

An interferogram is formed by multiplying the complex value of a pixel in one image by the complex conjugate of the corresponding pixel in the second image of the interferometric pair. It is the phase of the complex value in the interferogram that contains the deformation signal. However, the interferometric phase measurement suffers from two complicating factors that must be addressed before the deformation signal can be extracted. First, the interferometric phase encodes not only the surface deformation signal, but also a measurement of the surface topography whenever the baseline is non-zero. By simulating an interferogram using a digital elevation model (DEM) of the scene the topographic signature component of the interferometric phase can be predicted and removed. Also, the interferometric phase is only measured modulo 2π, which represents one half wavelength (12 cm) of surface deformation. Since the deformation signal can be many multiples of 2π a two dimensional phase unwrapping procedure is applied to get an unambiguous deformation measurement. After geocoding data from multiple repeat-passes, they are combined to reduce thermal and atmospheric noise, or, if the data are collected from multiple vantages, we reconstruct the three dimensional deformation vector. A single interferometric measurement is only sensitive to deformation in the line-of-sight direction.

We tested the image formation algorithms using simulated data from either a point target simulator and from reformatted AIRSAR data. The point target simulator simulates the science and motion data for one to hundreds of discrete point scatterers distributed over a scene from which detailed image formation metrics are extracted and compared to requirements. The point target simulator includes detailed modeling of the electronically scanned antenna and onboard steering algorithms. Thus, the point target simulator allows rigorous testing of new processing algorithms associated with the electronically scanned antenna prior to actual flight testing. Further testing of the image formation algorithm is done by reformatting real SAR data collected from the AIRSAR system and converting it into UAVSAR data formats. Although the electronic scanning aspects of UAVSAR cannot be tested with reformatted AIRSAR data, subsequent processing algorithms requiring distributed target data (e.g. baseline estimation refinement) can be tested using single look complex data generated this way. Figure 10 shows an image of Mt. St. Helens processed through the UAVSAR image formation processor using reformatted AIRSAR data.

The motion, image and interferometric processing software are hosted on an SGI Altix 350 computer with 16 processors and 32 GB of RAM. The Altix has 25 TB of online disk storage coupled with a Cybernetics LTO-3 8-slot tape library for access to archived raw or processed data. The software can process two fully polarimetric data sets (8 channels) of data simultaneously to support polarimetric interferometric applications such as three-dimensional vegetation structure estimation.

Ultimately, the goal of the UAVSAR system is not simply making surface deformation measurements, but using these measurements to achieve a better understanding of the underlying physics of solid earth processes. Geophysical inversion algorithms that take the deformation maps and invert for

Fig. 10. *L-Band AIRSAR data of Mt. St. Helens that has been reformatted into the UAVSAR data format and processed through the UAVSAR image processor.*

quantities of interest, e.g. fault depth and orientation for seismic sources or depth and volume for volcanoes, are being developed by Stanford University as an integral component of the ground data system. Future application of UAVSAR might include support in response to natural hazards, such as an earthquake, as these algorithms and the system mature.

III. Planned Flight Testing of Instrument

UAVSAR has a very tight flight testing schedule that is organized into three phases. The first phase is primarily dedicated to engineering checkout of the instrument and the Precision Autopilot Algorithm. These flights are designed to verify that the radar can collect good science data in a variety of modes that cover the span of the adjustable radar parameters. Particular emphasis is placed on verifying the stability and performance of the actively scanned array and of the automatic steering algorithms designed to maintain pointing within the required tolerances for repeat-pass interferometry. It is expected that this process will take approximately four flights, that will take place over the Rosamond Lake Bed in the Mojave Desert of California where we have a surveyed array of 22 trihedral corner reflectors.

The second phase of flight testing is designed to characterize and calibrate the radar instrument and to verify that performance is within requirements for the instrument. Characterization of the instrument entails establishing how much variation in phase or amplitude the radar undergoes as a function of temperature, antenna steering angle, mode or other adjustable radar parameters. The observed variations are compared with *a priori* expected variations, and when differences exceed acceptable tolerances, calibration data is collected and used to generate appropriate correction curves. Radar parameters to be calibrated include electronic timing delays, antenna phase center corrections, attitude angle biases and overall radiometric correction coefficients. The first series of repeat pass flights will be conducted in this phase to verify our motion reconstruction, repeat pass image formation and differential interferogram generation algorithms. Image formation and interferogram quality metrics such as resolution, Integrated Sidelobe Ratio (ISLR) and Peak Sidelobe Ratio (PSLR) as well as phase residuals in differential interferograms are computed using data collected over the corner reflectors deployed at Rosamond Lake Bed.

TABLE II
Flight Test Plans

Flight Number	Description
Flights 1-4	Engineering checkout flights designed to verify basic functionality of the instrument, e.g. manual versus automatic modes, PRF, pulse width and gain settings and the electronic steering of the antenna. Flights will be conducted over the Rosamond Lakebed in California.
Flights 5-10	These flights are designed to collect characterization and calibration data for the instrument. Data is collected to geometrically and radiometrically calibrate the imagery, to verify the repeat motion compensation algorithms, and characterize the temporal stability of the instrument. These flights will be primarily conducted over the Rosamond Lakebed in California.
Flights 11-20	These flights will collect repeat pass radar interferometric data for several time scales and locations to verify the deformation science goals of the instrument. Sites being considered for these observations include Parkfield, CA, Lost Hills, CA, Long Valley, CA, Mt St Helens in Washington State and Kilaeua Volcano on the island of Hawaii. These sites represent seismic, volcano and anthropogenic sources of deformation.

The final phase of testing is devoted to repeat pass radar interferometric experiments over regions of scientific interest. Initial test sites have been chosen to look for surface deformation signatures in seismically active regions, volcanoes and at a site where anthropogenically induced surface deformation is occurring. Seismic activity along the San Andreas Fault in California is of great interest due to the potential for a major earthquake occurring along this fault. Parkfield, California, is a well studied and instrumented site along the San Andreas fault ([6], [3]) that is well suited for initial seismic studies with the UAVSAR instrument. Lost Hills, California, is a site that has been studied using spaceborne interferometry as a source of anthropogenically induced surface deformation resulting from oil pumping. Volcanic sites of potential interest include Long Valley ([9],[2]), California, Mt. St. Helens, Washington, and Kilaeua, Hawaii ([8]) where active deformation has been occurring in recent years. Selection of a volcanic site will depend on the amount of recent activity at these sites and logistical considerations of fitting the observation into the flight testing schedule.

Table II provides a summary of the major objectives in each of the three flight testing phases.

IV. Conclusion

Development of the UAVSAR instrument is nearing completion and we are now starting its flight test program. This system will be the first civilian SAR to incorporate an electronically scanned array and is expected to provide a robust repeat-pass interferometric mapping capability to the science community. The system has been designed with portability and

extensibility as primary factors. Initial flights and laboratory testing of the instrument indicate that it will meet its instrument and science requirements. Flight tests over the next year will provide the first science data from UAVSAR and will produce surface deformation maps with increased temporal and spatial resolution compared with existing spaceborne sensors. With future upgrades, UAVSAR will be able to support the science community beyond solid earth, cryosphere, and land cover applications. The UAVSAR website, [1], contains additional information on UAVSAR, imagery and other data products will be posted as they become available.

ACKNOWLEDGMENT

A number of organizations have been integral to the development of the UAVSAR system. We would especially like to thank NASA Dryden for their overall leadership in the aircraft modifications, installation of the pod and development of the Precision Autopilot capability; Total Aircraft Services for the pod design and G-III modifications; REMEC Defense and Space for the development and supplying of the L-band TR modules; and Artemis for the design and manufacture of the modules in the RF subsystem. This research was conducted at the Jet Propulsion Laboratory, California Institute of Technology, under contract with the National Aeronautics and Space Administration.

Reference herein to any specific commercial product, process, or service by trade name, trademark, manufacturer, or otherwise, does not constitute or imply its endorsement by the United States Government or the Jet Propulsion Laboratory, California Institute of Technology.

REFERENCES

[1] http://uavsar.jpl.nasa.gov.

[2] M. Battaglia, P. Segall, and C. Roberts. The mechanics of unrest at Long Valley caldera, California. 2. Constraining the nature of the source using geodetic and micro-gravity data. *Journal of Volcanology and Geothermal Research*, 127, 2003.

[3] K.L. Feigl, D.C. Agnew, Y. Bock, D. Dong, A. Donnellan, B.H. Hager, T.A. Herring, D.D. Jackson, T.H. Jordan, and R.W. King. Space geodetic measurement of crustal deformation in central and southern California, 1984-1992. *Journal of Geophysical Research*, 98, December 1993.

[4] R. Kwok and W.T.K. Johnson. Block adaptive quantization of Magellan SAR data. *IEEE Transactions on Geoscience and Remote Sensing*, 27(4):375–383, July 1989.

[5] James Lee, Brian Strovers, and Victor Lin. C-20A/GIII Precision Autopilot development in support of NASAs UAVSAR program. In *Proceeding of the NASA Science Technology Conference 2007*, Greenbelt, Maryland, June 2007. NASA.

[6] P. Rosen, C. Werner, E. Fielding, S. Hensley, S. Buckley, and P. Vincent. Aseismic creep along the San Andreas Fault northwest of Parkfield, California, measured by radar interferometry. *Geophysical Research Letters*, 25:825–828, 1998.

[7] P. A. Rosen, S. Hensley, I. R. Joughin, F. K. Li, S. N Madsen, E. Rodriquez, and R. M. Goldstein. Synthetic Aperture Radar Interferometry. *Proc. IEEE*, 88:333–382, 2000.

[8] P. A. Rosen, S. Hensley, H. A. Zebker, F. H. Webb, and E. J. Fielding. Surface deformation and coherence measurements of Kilauea Volcano, Hawaii, from SIR-C radar interferometry. *Journal of Geophysical Research*, 268:1333–1336, 1996.

[9] Michael L. Sorey, Vicki S. McConnell, and Evelyn Roeloffs. Summary of recent research in Long Valley Caldera, California. *Journal of Volcanology and Geothermal Research*, 127, 2003.